

# A test of MOND and Emergent Gravity with SMACS J0723.3-7327 using eROSITA observations

Ambica Govind\* and Shantanu Desai†

*Department of Physics, Indian Institute of Technology, Hyderabad, Kandi, Telangana-502284 India*

We implement a test of MOND and Verlinde's Emergent Gravity using the galaxy cluster SMACS J0723-7327, which has been recently imaged using the eROSITA X-ray telescope as well as with JWST. We test MOND using two independent methods. The first method involves comparing the dynamical MOND mass and baryonic mass, while the second method entails a comparison of the MOND-estimated temperature with the observed temperature. We then compare the unseen mass predicted by Emergent Gravity with the estimated dark matter mass. We find that MOND is able to explain the mass discrepancy at large radii but not in the central regions. The observed temperature profile is also in slight disagreement with that in the MOND paradigm. Likewise the Emergent Gravity Theory shows a marginal discrepancy in accurately accounting for the dynamical mass in the inner regions. Our results are qualitatively consistent with the earlier tests on other clusters.

## I. INTRODUCTION

One of the key ingredients of the standard  $\Lambda$ CDM Concordance model of the universe [1] is Cold Dark matter which constitutes about 25% of the total mass-energy budget. This cold dark matter component is known to be non-baryonic and decouples from the remaining components of the universe, while moving at non-relativistic velocities [2–4]. Although, this  $\Lambda$ CDM model agrees remarkably well with observational data at large-scales [5], there is no laboratory evidence for any cold dark matter candidate, despite over three decades of searches via underground dark matter laboratory searches [6] or indirect dark matter searches through annihilation products [7, 8] or accelerator based searches [9]. We still do not know answers to even rudimentary questions about the CDM particle as to whether it is a fermion or boson, and also on whether it is a thermal or a non-thermal relic.

Therefore, one possible alternative to the above standard picture, which obviates the need for dark matter, is the modified Newtonian Dynamics (MOND) paradigm [10]. One can think of MOND as a theoretical extension of Newtonian dynamics in the low acceleration limit, i.e. for acceleration below some constant value  $a_0 \approx 10^{-10} \text{ms}^{-2}$ , where  $a_0$  is referred to as Milgrom's constant. Milgrom established a smooth transition between the dark matter dominated and the Newtonian regimes i.e.  $g \gg a_0$  and  $g \ll a_0$  using the formula

$$\mu\left(\frac{g}{a_0}\right) \mathbf{g} = \mathbf{g}_N, \quad (1)$$

where the interpolation function ( $\mu(x)$ ) is given by,  $\mu(x) \rightarrow 1$  for  $x \gg 1$  and  $\mu(x) \rightarrow x$  for  $x \ll 1$ . Many examples of such MOND interpolation functions can be found in Famaey and McGaugh [11]. The MOND paradigm relates the observed gravitational acceleration  $g$  and the Newtonian acceleration calculated from only the baryonic mass ( $g_{bar}$ ), i.e. for acceleration above  $a_0$ ,  $g_{obs} \approx g_{bar}$  and for acceleration below the value,  $g_{obs} \propto g_{bar}^{1/2}$  [11].

The MOND paradigm can also explain some of the regularities and deterministic scaling relations at galactic scales such as the Radial acceleration relation (RAR) [12], constancy of halo dark matter surface density [13], baryonic Tully-Fisher relation [11]. These successes cannot be trivially reproduced by the standard  $\Lambda$ CDM model, although some of the latest  $\Lambda$ CDM simulations can reproduce the observed RAR [14] and the constancy of dark matter surface density [15]. All the empirical successes of MOND which cannot be explained within  $\Lambda$ CDM have recently been reviewed in [16]. Of course, there are also some tensions of MOND with observations of our own galaxy, where it is difficult to predict the observed decline in rotation curve at large distances [17].

However, it has been known since a long time, that MOND (in its original form) does not work well for relaxed galaxy clusters in hydrostatic equilibrium [18–25]. For relaxed galaxy clusters, MOND has been tested using two different methods in literature. In the first of these methods, the dynamical MOND masses for clusters have been calculated using a modified equation of hydrostatic equilibrium and found to be much larger than the baryonic mass,

---

\*ep21btech11007@iith.ac.in

†shntn05@gmail.com

consisting of hot diffuse gas and stars [18, 21–23]. Using this method, the dynamical MOND mass was found to be larger than the observed baryonic mass [18, 21–23]. Alternately, MOND has also been tested using the usual (Newtonian) equation of hydrostatic equilibrium, but plugging the MONDian formula for the acceleration, in order to derive the resulting temperature profile [20]. This estimated temperature profile was found to be much smaller than the observed temperature profiles, thus providing a strong challenge for MOND [20]. Therefore, the conclusion is that even within the MOND paradigm, galaxy clusters have unaccounted for missing mass. However, these works have not carried out a detailed error analysis to ascertain the statistical significance of the discrepancies. Therefore, it is important to redo these tests with new observations, for which a detailed characterization of the error budget is available.

Recently, observational tests of some of the regularities found at galactic scales (which led to the MOND paradigm) such as the RAR and constancy of dark matter surface density have also been done on cluster scales. These results showed that the acceleration scale and halo surface density were found to be higher compared to galactic scales and different among cluster samples, implying that the RAR cannot be universal [26–34]. Many relativistic theories of MOND are also in tension due to the coincident gravitational wave and EM observations from GW 170817 [35].

Recently, a new modified theory of gravity has been proposed which combines the success of MOND at galactic scales with that of  $\Lambda$ CDM at cosmological scales [36]. This model is known as Entropic or Emergent gravity. Emergent Gravity asserts that spacetime and gravity emerge together from the entanglement structure of an underlying microscopic theory. Vacuum excitations impart entropy content to space that manifests itself as dark energy. Baryonic matter displaces this dark energy and causes an elastic restoring force on matter—the additional ‘dark gravity’ hitherto posited to be the effect of dark matter in  $\Lambda$ CDM. A large number of tests of Emergent Gravity have been done using galaxy clusters [37–41], dwarf galaxies [42], dwarf spheroidal galaxies [43] and spiral galaxies [44, 45], early-type galaxies [46], weak galaxy-galaxy lensing [47–49]. The results from these works have provided mixed results for Emergent Gravity with some observations in agreement [43, 45, 47, 48], whereas others in tension [42, 44, 49], while results with clusters show both an agreement and disagreement depending on the distance from the cluster center [37–41].

In 2019, the eROSITA satellite was launched, which will carry out an all-sky X-ray survey to discover new galaxy clusters and map out their properties with unprecedented precision and at the end of its survey will achieve a sensitivity of 25 times better than the ROSAT mission [50]. The eROSITA survey has already discovered a large number of galaxy clusters and has done a detailed characterization of X-ray gas properties of these clusters including the error budget [51]. In this work, we revisit some of the tests of MOND and Emergent Gravity previously carried out with relaxed cluster samples using one such galaxy cluster, which has been imaged with eROSITA and other telescopes in X-ray and optical, namely SMACS J0723.3-7327.

The manuscript is structured as follows. The dataset used for the analysis is described in Sect. II. Our results for tests of MOND are outlined in Sect. III. Our tests of Emergent Gravity can be found in Sect. IV. We conclude in Sect. V.

## II. DATASET USED FOR ANALYSIS

For this analysis, we use multi-wavelength observations of SMACS J0723.3-7327 (J0723 hereafter) described in [52] (L22, hereafter). J0723 is a massive galaxy cluster located at a redshift  $z = 0.39$  and with  $M_{500} = 9.8 \pm 5.1 \times 10^{14} M_{\odot}$  and temperature given by  $kT_{500} \sim 7$  keV. This cluster has also been previously detected in X-Rays by ROSAT, Chandra and XMM-Newton, in SZ by Planck and was the first lensing cluster observed by the James Webb space telescope. The hydrostatic mass for J0723 is also in agreement with the lensing mass indicating that there is no hydrostatic bias for this cluster [53]. For this work we used X-ray observations of J0723 from eROSITA using their all-sky survey data from December 2019 to February 2022 with a total exposure time of 4.4 ks. It was scanned five times during the first five eROSITA all-sky surveys. In addition, archival Chandra observations (from April 2014) were also used to constrain the temperature profile in the cluster center. More details on the observations and data reduction can be found in L22. The temperature profiles were estimated by combining the Chandra and eROSITA data. The electron density profiles were provided separately for both Chandra and eROSITA. L22 find that the measurements of temperature, gas mass and density as well as the hydrostatic mass is consistent between Chandra and eROSITA within  $R_{2500}$ . Along with the best-fit parameters for temperature and pressure,  $1\sigma$  error bars have also been provided for all the free parameters in L22.

### III. TESTING MOND

We test MOND for J0723 using two different methods. In the first method we compare the dynamical mass in the MOND picture to the observationally inferred baryonic mass. In the second method, we compare the observed temperature profile to that predicted by MOND.

#### A. Comparison of dynamical and observed masses

In order to test MOND with this relaxed cluster, we follow the same methodology as in [21]. We assume the intracluster medium to be an isotropic isothermal sphere characterized by the equation of hydrostatic equilibrium (HSE):

$$\frac{dP}{dr} = -\rho g, \quad (2)$$

where  $P$  denotes the pressure,  $\rho$  being the density, and  $g$  is the observed gravitational acceleration. Since the hydrostatic mass agrees with the lensing mass, the HSE assumption is justified. To test MOND, we plug the value of  $g$  from Eq. 1. Here, we use  $a_0 = 1.2 \times 10^{-8} \text{ cm/s}^2$ , which is the critical acceleration that demarcates the MOND regime from the Newtonian regime. The MOND interpolation function we use here is as follows [11]:

$$\mu(x) = \frac{x}{\sqrt{1+x^2}} \quad (3)$$

We then obtain the observed acceleration  $g$  from Eq 2 and assuming an ideal gas equation of state:

$$g = -\frac{1}{\rho} \frac{dp}{dr} = -\frac{kT}{f m_p r} \left[ \frac{d \ln \rho}{d \ln r} + \frac{d \ln T}{d \ln r} \right], \quad (4)$$

and the dynamical mass in the Newtonian regime is given by [54]:

$$M_N = -\frac{kTr}{Gf m_p} \left[ \frac{d \ln \rho}{d \ln r} + \frac{d \ln T}{d \ln r} \right] \quad (5)$$

If we further posit the interpolation function to be of the form as in Eq. 3, the dynamical mass in MOND regime comes out to be:

$$M_m = \frac{M_N}{\sqrt{1 + \left(\frac{a_0}{g}\right)^2}} \quad (6)$$

In order to use Eq 5, we require the radial temperature and density profiles of the cluster. For this purpose we use the profiles provided in L22. The radial temperature profile of J0723 was fit to the following model originally used in [55] to model Chandra X-ray cluster sample:

$$T(r) = T_0 \frac{(r/r_{cool})^{a_{cool}} + T_{min}/T_0}{(r/r_{cool})^{a_{cool}} + 1} \frac{(r/r_t)^{-a}}{\left[1 + (r/r_t)^b\right]^{c/b}} \quad (7)$$

L22 used the gas number density profiles also from [55], which is an augmented version of the  $\beta$ -profile [56] but without the second  $\beta$ -component:

$$n_p n_e = n_0^2 \cdot \frac{(r/r_c)^{-\alpha}}{(1 + r^2/r_c^2)^{3\beta - \alpha/2}} \frac{1}{(1 + r\gamma/r_s\gamma)^{\epsilon/\gamma}}, \quad (8)$$

and the corresponding gas mass density is calculated using

$$\rho_{gas} = 1.624 m_p \sqrt{n_p n_e} \quad (9)$$

L22 finds that the above model can explain its observational profiles well, where the Markov Chain Monte Carlo fits to the parameters can be found.

The above relations are employed to calculate the dynamical mass in the Newtonian and thereby in the MOND picture. We then calculate the baryonic mass ( $M_{baryon}$ ) which is given by the sum of gas ( $M_{gas}$ ) and star mass ( $M_{\star}$ ). We calculate the mass of the gas within a radius  $r$  (assuming spherical symmetry) to be:

$$M_{gas}(r) = 4\pi \int_0^r r^2 \rho_{gas}(r) dr \quad (10)$$

Similar to our work on tests of linearity of dark matter to baryonic mass [57], we used the estimate of the stellar mass from the stellar-gas mass relations derived in [58]:

$$M_{\star}(r) = 4 \times 10^{12} M_{\odot} \times \left( \frac{M_{gas}(r)}{5.7 \times 10^{13} M_{\odot}} \right)^{0.60 \pm 0.10} \quad (11)$$

This relation was obtained using a sample of 91 SPT-SZ clusters detected up to redshift of 1.3 and includes contributions from the brightest cluster galaxy as well as cluster member galaxies within  $r_{500}$ .

In order to test MOND, we compare the dynamical mass of the cluster within MOND with the baryonic mass and if they agree within the error bars, then it would show that MOND prescription can adequately describe this cluster. We calculate both the baryonic and MOND dynamical masses at 1000 radii uniformly distributed between the cluster center and  $r_{500}$ . The errors in the MOND and baryonic mass were obtained through error propagation, using the  $1\sigma$  error bars provided in L22 for all the free parameters of the gas and temperature profiles. This comparison of the MOND dynamical mass and observed baryonic mass can be found in Fig. 1, where we show masses corresponding to 11 radii. At low radii, the MOND masses are much higher in magnitude than the total baryonic mass, with a maximum disparity of  $29\sigma$ . The disparity quickly reduces with the radius and at  $r \approx 1000\text{kpc}$ , the MOND dynamical mass is consistent within  $1\sigma$  with the baryonic mass, indicating that MOND is able to viably explain cluster dynamics at this scale. Therefore, although MOND can be considered workable at these large radii, there still remains a large amount of “missing mass” close to the cluster center at around  $29\sigma$ , which is unaccounted for by MOND.

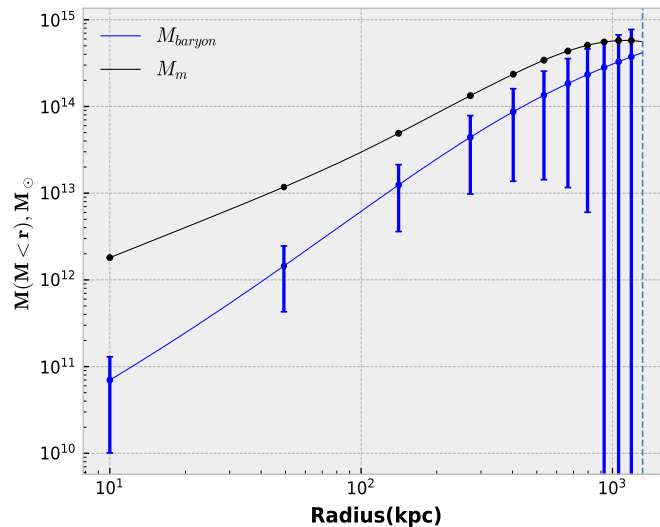


FIG. 1: A comparison of the dynamical mass in the MOND and Newtonian regime with the baryonic mass observed from eROSITA as a function of distance from the cluster center plotted until  $r_{500}$ . The error bars indicate the uncertainties as calculated by error propagation. The uncertainty in the baryonic mass is pronounced at large radii due to errors in  $n_0$  and  $r_c$ .

## B. Temperature Profiles

We now test MOND using the same methodology as in [20]. Here, instead of comparing the dynamical MOND and baryonic mass, we solve for the temperature profile, by using the MONDian acceleration in HSE, and then compare

that to the observed temperature profile. We briefly recap this procedure. In the limit  $g \ll a_0$ , Eq. 4 can be rearranged as:

$$\frac{d \ln \rho}{d \ln r} + \frac{d \ln T}{d \ln r} = -\frac{g f m_p r}{kT} = -\frac{\sqrt{g_N a_0} f m_p r}{kT} = -\frac{\sqrt{G M_m a_0} f m_p}{kT} \quad (12)$$

To calculate the temperature profile in the MOND and hydrostatic equilibrium scenario, we numerically calculate  $T(r)$  from Eq. 12 given the observed  $\rho(r)$  (where we used the eROSITA estimated parameters) and the dynamical mass in the MOND Scenario. The calculation is done via a fourth-order Runge-Kutta method with the initial condition that  $T(10 \text{ kpc})$  in Eq. 12 is equal to the observed temperature. Once again, we show the observed and MOND-estimated temperature at about 10 radii from cluster center until  $r_{500}$ . This plot can be seen in Fig. 2. Although both the temperatures agree (by construction) at 10 kpc, we find that MOND predicts a higher temperature than the observed temperature at all radii, with the disparity only increasing with  $r$ . We find a maximum difference of  $1.9\sigma$  at a radius of 82 kpc and at  $r_{500}$ , the discrepancy is about  $1.6\sigma$ . Therefore, we find using this method also we see a discrepancy in the observed and estimated temperature profiles, although it is not as pronounced as the analysis in Sect. III A.

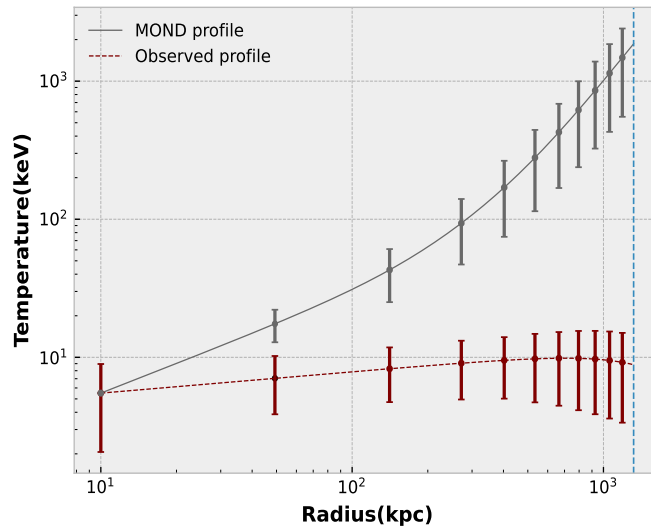


FIG. 2: A comparison of the observed temperature profile against the numerically calculated temperature profile in the MOND framework plotted until  $r_{500}$ . The uncertainties are calculated using error propagation from the six observed density parameters to the numerically calculated temperature.

#### IV. TESTING EMERGENT GRAVITY

In order to test Emergent Gravity, we follow the same prescription as [37], which derived the following relation between the baryonic mass and the emergent “dark matter” which arises due to elastic response resulting from the entropy displacement:

$$M_{DM,EG}^2(r) = \frac{cH_0}{6G} r^2 M_{baryon}(r) (1 + 3\delta_B) \quad (13)$$

where  $\delta_B = \rho_B(r)/\bar{\rho}_B$ , with  $\bar{\rho}_B = M_{baryon}(r)/V(< r)$  denoting the mean baryon density within a spherical volume of radius  $r$ . In our test we calculate the mass of the emergent dark matter component and compare it with the Newtonian estimate of dark matter given by  $M_N - M_{baryon}$ . The Newtonian and baryonic mass are estimated in the same way as in Sect. III A:

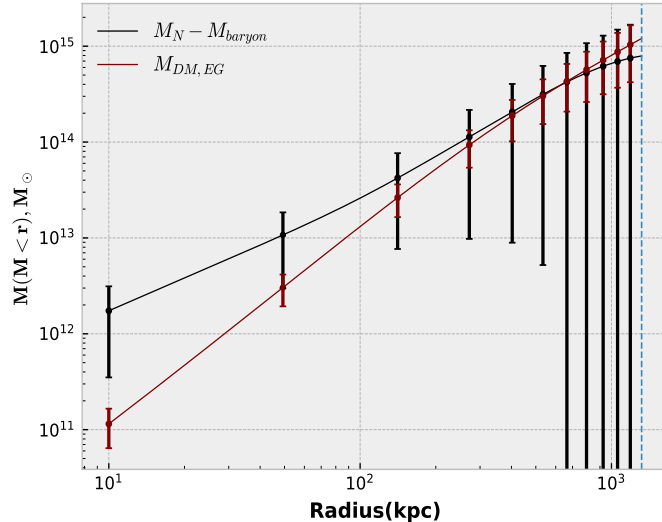


FIG. 3: A comparison of the mass deficit with the dark matter estimate in the Emergent Gravity formulation until  $r_{500}$ . The error bars show the uncertainties calculated by error propagation. The mass deficit has a very high uncertainty as the error contribution from each of the 14 parameters adds up collectively.

A comparison of the two can be found in Fig. 3. From Fig 3, we see that the dark matter estimations from the Emergent Gravity Theory is unable to account for the mass deficit at smaller radii (until about 50 kpc), but is able to explain it well starting from 100 kpc and beyond. The discrepancy between the two at 10 kpc is about  $1.2 \sigma$ . Therefore, we find that the EG paradigm is mostly consistent with observations except close to the center where it shows a marginal discrepancy.

## V. CONCLUSIONS

In this work we have used X-Ray observations from eROSITA to test two modified gravity theories (namely MOND and Emergent Gravity) which dispense with the need for dark matter, using the cluster J0723 observed recently with eROSITA and also JWST and discussed in L22. We tested MOND using two independent methods. In the first method, we compared the dynamical mass in MOND with the total baryonic mass. In the second method, we compared the MOND inferred temperature profile with the observed temperature. In order to test Emergent Gravity, we compared the excess mass predicted with Emergent Gravity with the observed Newtonian missing mass. For all the above calculations, we used temperature and density profiles provided in L22. Our conclusions are as follows:

- The first test renders MOND successful far away from the cluster center ( $\approx 1000$  kpc), but not close to it, requiring a residual ‘missing mass’ with the largest discrepancy amounting to  $29\sigma$  at 10 kpc.
- The second test implies that MOND predicts a temperature profile much different than what is observed with a higher temperature at all radii with the largest discrepancy of about  $1.9\sigma$ .
- The third test conveys that Emergent Gravity, akin to MOND is unable to explain the observed mass deficit using this emergent dark matter at small radii with a slight discrepancy of about  $1.2\sigma$  at around 10 kpc. It is however in agreement with observations for  $r \geq 50$  kpc. At larger radii ( $> 700$  kpc), Emergent Gravity slightly overestimates this quantity. This is consistent with earlier studies.

The theories can be reconciled with observations only when there is evidence of missing baryons close to the cluster center, additional non-baryonic components such as neutrinos [21] or one needs non-local versions of MOND [59, 60] or some of the most recent relativistic versions proposed in [61]. Efforts from various fields in the scientific community are underway to address these, in the form of precise observations, dark matter searches and theoretical development. On the observational side, we expect an improvement of results with better quality of X-Ray data powered by more

sophisticated missions such as Athena [62] or eXTP [63] to be deployed within the next decade. This data would render more precise tests of MOND and Emergent Gravity, among others.

- 
- [1] B. Ratra and M. S. Vogeley, *PASP* **120**, 235 (2008), 0706.1565.
- [2] G. Jungman, M. Kamionkowski, and K. Griest, *Physics Reports* **267**, 195 (1996), hep-ph/9506380.
- [3] G. Bertone, D. Hooper, and J. Silk, *Physics Reports* **405**, 279 (2005), hep-ph/0404175.
- [4] A. Bosma, arXiv e-prints arXiv:2309.06390 (2023), 2309.06390.
- [5] P. Ade et al. (Planck), *Astron. Astrophys.* **594**, A13 (2016), 1502.01589.
- [6] D. Merritt, *Studies in the History and Philosophy of Modern Physics* **57**, 41 (2017), 1703.02389.
- [7] J. M. Gaskins, *Contemporary Physics* **57**, 496 (2016), 1604.00014.
- [8] S. Desai, Y. Ashie, S. Fukuda, Y. Fukuda, K. Ishihara, Y. Itow, Y. Koshio, A. Minamino, M. Miura, S. Moriyama, et al., *Phys. Rev. D* **70**, 083523 (2004), hep-ex/0404025.
- [9] A. Canepa, *Reviews in Physics* **4**, 100033 (2019).
- [10] M. Milgrom, *Astrophys. J.* **270**, 365 (1983).
- [11] B. Famaey and S. S. McGaugh, *Living Reviews in Relativity* **15**, 10 (2012), 1112.3960.
- [12] S. S. McGaugh, F. Lelli, and J. M. Schombert, *Phys. Rev. Lett.* **117**, 201101 (2016), 1609.05917.
- [13] F. Donato, G. Gentile, P. Salucci, C. Frigerio Martins, M. I. Wilkinson, G. Gilmore, E. K. Grebel, A. Koch, and R. Wyse, *Mon. Not. R. Astron. Soc.* **397**, 1169 (2009), 0904.4054.
- [14] A. Paranjape and R. K. Sheth, *Mon. Not. R. Astron. Soc.* **507**, 632 (2021), 2102.13116.
- [15] K. Gopika, S. Desai, and A. Paranjape, *Mon. Not. R. Astron. Soc.* **523**, 1718 (2023), 2303.12859.
- [16] I. Banik and H. Zhao, *Symmetry* **14**, 1331 (2022), 2110.06936.
- [17] M. H. Chan and K. C. Law, *Astrophys. J.* **957**, 24 (2023).
- [18] L. S. The and S. D. M. White, *Astron. J.* **95**, 1642 (1988).
- [19] D. Gerbal, F. Durret, M. Lachieze-Rey, and G. Lima-Neto, *Astron. & Astrophys.* **262**, 395 (1992).
- [20] A. Aguirre, J. Schaye, and E. Quataert, *Astrophys. J.* **561**, 550 (2001), astro-ph/0105184.
- [21] R. H. Sanders, *Mon. Not. R. Astron. Soc.* **342**, 901 (2003), astro-ph/0212293.
- [22] G. W. Angus, B. Famaey, and D. A. Buote, *Mon. Not. R. Astron. Soc.* **387**, 1470 (2008), 0709.0108.
- [23] E. Pointecouteau and J. Silk, *Mon. Not. R. Astron. Soc.* **364**, 654 (2005), astro-ph/0505017.
- [24] P. Natarajan and H. Zhao, *Mon. Not. R. Astron. Soc.* **389**, 250 (2008), 0806.3080.
- [25] S. Seeram and S. Desai, *Journal of Astrophysics and Astronomy* **42**, 3 (2021).
- [26] Y. Tian, K. Umetsu, C.-M. Ko, M. Donahue, and I. N. Chiu, *Astrophys. J.* **896**, 70 (2020), 2001.08340.
- [27] M. H. Chan and A. Del Popolo, *Mon. Not. R. Astron. Soc.* p. 218 (2020), 2001.06141.
- [28] S. Pradyumna, S. Gupta, S. Seeram, and S. Desai, *Physics of the Dark Universe* **31**, 100765 (2021).
- [29] S. Pradyumna and S. Desai, *Physics of the Dark Universe* **33**, 100854 (2021), 2107.05845.
- [30] D. Eckert, S. Ettori, E. Pointecouteau, R. F. J. van der Burg, and S. I. Loubser, *Astron. & Astrophys.* **662**, A123 (2022), 2205.01110.
- [31] M. H. Chan and K. C. Law, *Phys. Rev. D* **105**, 083003 (2022), 2203.15217.
- [32] M. H. Chan, *Mon. Not. R. Astron. Soc.* **442**, L14 (2014), 1403.4352.
- [33] K. Gopika and S. Desai, *Physics of the Dark Universe* **30**, 100707 (2020), 2006.12320.
- [34] K. Gopika and S. Desai, *Physics of the Dark Universe* **33**, 100874 (2021), 2106.07294.
- [35] S. Boran, S. Desai, E. O. Kahya, and R. P. Woodard, *Phys. Rev. D* **97**, 041501 (2018), 1710.06168.
- [36] E. P. Verlinde, *SciPost Physics* **2**, 016 (2017), 1611.02269.
- [37] S. Ettori, V. Ghirardini, D. Eckert, F. Dubath, and E. Pointecouteau, *Mon. Not. R. Astron. Soc.* **470**, L29 (2017), 1612.07288.
- [38] S. Ettori, V. Ghirardini, D. Eckert, E. Pointecouteau, F. Gastaldello, M. Sereno, M. Gaspari, S. Ghizzardi, M. Roncarelli, and M. Rossetti, *Astron. & Astrophys.* **621**, A39 (2019), 1805.00035.
- [39] V. Halenka and C. J. Miller, *Phys. Rev. D* **102**, 084007 (2020), 1807.01689.
- [40] A. Tamosiunas, D. Bacon, K. Koyama, and R. C. Nichol, *JCAP* **2019**, 053 (2019), 1901.05505.
- [41] J. A. ZuHone and J. Sims, *Astrophys. J.* **880**, 145 (2019), 1905.03832.
- [42] K. Pardo, *JCAP* **2020**, 012 (2020), 1706.00785.
- [43] A. Diez-Tejedor, A. X. Gonzalez-Morales, and G. Niz, *Mon. Not. R. Astron. Soc.* **477**, 1285 (2018), 1612.06282.
- [44] F. Lelli, S. S. McGaugh, and J. M. Schombert, *Mon. Not. R. Astron. Soc.* **468**, L68 (2017), 1702.04355.
- [45] Y. Yoon, J.-C. Park, and H. S. Hwang, *Classical and Quantum Gravity* **40**, 02LT01 (2023), 2206.11685.
- [46] C. Tortora, L. V. E. Koopmans, N. R. Napolitano, and E. A. Valentijn, *Mon. Not. R. Astron. Soc.* **473**, 2324 (2018), 1702.08865.
- [47] M. M. Brouwer, M. R. Visser, A. Dvornik, H. Hoekstra, K. Kuijken, E. A. Valentijn, M. Bilicki, C. Blake, S. Brough, H. Buddelmeijer, et al., *Mon. Not. R. Astron. Soc.* **466**, 2547 (2017), 1612.03034.
- [48] M. M. Brouwer, K. A. Oman, E. A. Valentijn, M. Bilicki, C. Heymans, H. Hoekstra, N. R. Napolitano, N. Roy, C. Tortora, A. H. Wright, et al., *Astron. & Astrophys.* **650**, A113 (2021), 2106.11677.
- [49] W. Luo, J. Zhang, V. Halenka, X. Yang, S. More, C. J. Miller, L. Liu, and F. Shi, *Astrophys. J.* **914**, 96 (2021), 2003.09818.

- [50] P. Predehl, R. Andritschke, V. Arefiev, V. Babyshkin, O. Batanov, W. Becker, H. Böhringer, A. Bogomolov, T. Boller, K. Borm, et al., *Astron. & Astrophys.* **647**, A1 (2021), 2010.03477.
- [51] E. Bulbul, A. Liu, T. Pasini, J. Comparat, D. N. Hoang, M. Klein, V. Ghirardini, M. Salvato, A. Merloni, R. Seppi, et al., *Astron. & Astrophys.* **661**, A10 (2022), 2110.09544.
- [52] A. Liu, E. Bulbul, M. E. Ramos-Ceja, J. S. Sanders, V. Ghirardini, Y. E. Bahar, M. Yeung, E. Gattuzz, M. Freyberg, C. Garrel, et al., *Astron. & Astrophys.* **670**, A96 (2023), 2210.00633.
- [53] G. B. Caminha, S. H. Suyu, A. Mercurio, G. Brammer, P. Bergamini, A. Acebron, and E. Vanzella, *Astron. & Astrophys.* **666**, L9 (2022), 2207.07567.
- [54] C. L. Sarazin, *Reviews of Modern Physics* **58**, 1 (1986).
- [55] A. Vikhlinin, A. Kravtsov, W. Forman, C. Jones, M. Markevitch, S. Murray, and L. Van Speybroeck, *The Astrophysical Journal* **640**, 691 (2006).
- [56] A. Cavaliere and R. Fusco-Femiano, *Astron. & Astrophys.* **49**, 137 (1976).
- [57] V. Upadhyaya and S. Desai, *Physics of the Dark Universe* **40**, 101182 (2023), 2212.02326.
- [58] I. Chiu, J. Mohr, M. McDonald, S. Bocquet, S. Desai, M. Klein, H. Israel, M. Ashby, A. Stanford, B. Benson, et al., *Monthly Notices of the Royal Astronomical Society* **478**, 3072 (2018).
- [59] R. P. Woodard, *Canadian Journal of Physics* **93**, 242 (2015), 1403.6763.
- [60] M. Kim, M. H. Rahat, M. Sayeb, L. Tan, R. P. Woodard, and B. Xu, *Phys. Rev. D* **94**, 104009 (2016), 1608.07858.
- [61] C. Skordis and T. Złóśnik, *Phys. Rev. Lett.* **127**, 161302 (2021), 2007.00082.
- [62] D. Barret, A. Decourchelle, A. Fabian, M. Guainazzi, K. Nandra, R. Smith, and J.-W. den Herder, *Astronomische Nachrichten* **341**, 224 (2020), 1912.04615.
- [63] S. Zhang, A. Santangelo, M. Feroci, Y. Xu, F. Lu, Y. Chen, H. Feng, S. Zhang, S. Brandt, M. Hernanz, et al., *Science China Physics, Mechanics, and Astronomy* **62**, 29502 (2019), 1812.04020.